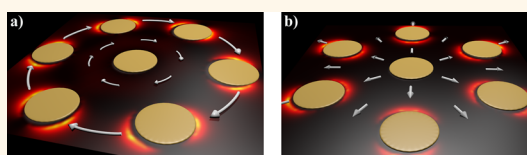


Near- and Far-Field Properties of Plasmonic Oligomers under Radially and Azimuthally Polarized Light Excitation

Avner Yanai,[†] Meir Grajower,[†] Gilad M. Lerman,[†] Mario Hentschel,^{‡,§} Harald Giessen,[‡] and Uriel Levy^{†,*}

[†]Department of Applied Physics, Hebrew University of Jerusalem, Jerusalem, 91904, Israel, [‡]4th Physics Institute and Research Center SCoPE, University of Stuttgart, Pfaffenwaldring 57, D-70569 Stuttgart, Germany, and [§]Max Planck Institute for Solid State Research, Heisenbergstrasse 1, D-70569 Stuttgart, Germany

ABSTRACT We present a comprehensive experimental and theoretical study on the near- and far-field properties of plasmonic oligomers using radially and azimuthally polarized excitation. These unconventional polarization states are perfectly matched to the high spatial symmetry of the oligomers and thus allow for the excitation of some of the highly symmetric eigenmodes of the structures, which cannot be excited by linearly polarized light. In particular, we study hexamer and heptamer structures and strikingly find very similar optical responses, as well as the absence of a Fano resonance. Furthermore, we investigate the near-field distributions of the oligomers using near-field scanning optical microscopy (NSOM). We observe significantly enhanced near-fields, which arise from efficient excitation of the highly symmetric eigenmodes by the radially and azimuthally polarized light fields. Our study opens up possibilities for tailored light–matter interaction, combining the design freedom of complex plasmonic structures with the remarkable properties of radially and azimuthally polarized light fields.



KEYWORDS: plasmons · radial and azimuthal polarization · near-field scanning optical microscopy · oligomers

In the past decade, the field of light–matter interaction manipulation at the nanoscale has witnessed many advances.^{1–3} With the use of artificial “plasmonic molecules” or “oligomers”, the ability to engineer the resonance spectrum of true nanoscale structures has been demonstrated.^{4–7} Moreover, these structures have been proven to be interesting for the study of the interplay between the supported modes,^{8–10} recently even demonstrating the excitation of toroidal modes.¹¹

In this paper, we study the interaction between oligomer clusters and cylindrical vector beams.¹² Each oligomer is made of a gold nanodisk, deposited on a SiO₂ substrate. We study two types of oligomer clusters. The first type, defined as the heptamer configuration, comprises seven nanodisks: six peripheral ones and one central. The second, defined as the hexamer configuration, consists of six peripheral disks only. Moreover, we study two polarization types of the incident beam, known as radial and azimuthal polarizations. These polarizations are of interest for nanoscale light–matter

interaction applications because of their ability to focus light to smaller spot sizes compared with linearly polarized beams.^{13–17} Moreover, these polarizations provide better matching between the polarization and structural symmetry of the studied nanostructures^{18–21} compared to linearly polarized light, as discussed next.

RESULTS AND DISCUSSIONS

Figure 1 illustrates a heptamer which is excited by (a) azimuthally and (b) radially polarized light. The gold circles correspond to the Au disks of the heptamer. Typical energy density distribution, represented by red/yellow colors, is superimposed on the geometrical structure. Polarization direction of the excitation beam is denoted by the white arrows. It is evident that the structure possesses C_6 symmetry; *i.e.*, it is invariant under rotation of $2\pi/6$ radians around the center of the structure. This symmetry also holds for the hexamer structures. The radial and azimuthal polarization illuminations exhibit C_∞ symmetry; *i.e.*, they are invariant under continuous rotation around the

* Address correspondence to ulevy@cc.huji.ac.il.

Received for review February 20, 2014 and accepted April 23, 2014.

Published online April 23, 2014
10.1021/nn501031t

© 2014 American Chemical Society

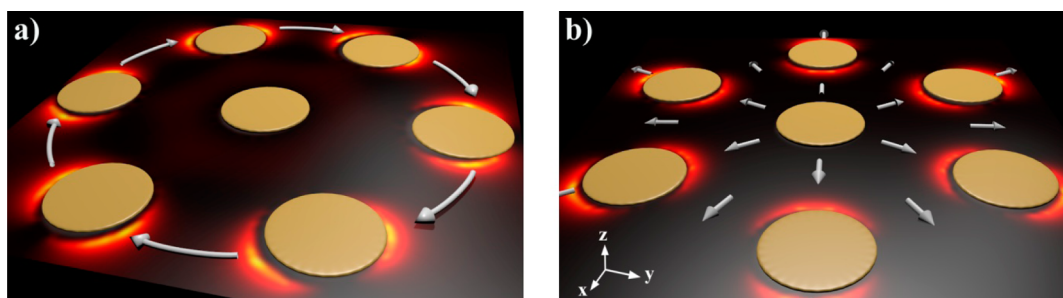


Figure 1. Illustration of an Au heptamer on top of a glass substrate excited with (a) azimuthal polarization and (b) radial polarization.

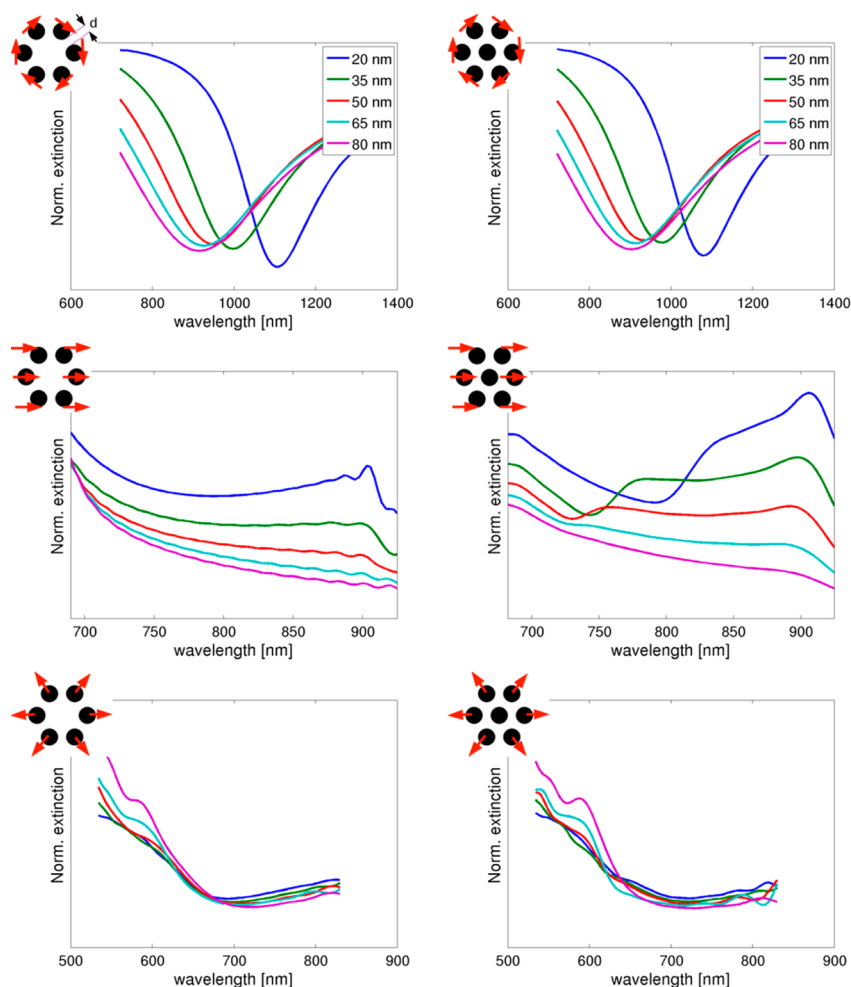


Figure 2. Extinction in arbitrary units as a function of wavelength for azimuthal, linear, and radial polarization illumination for hexamer and heptamer structures. Calculation has been performed for disk surface-to-surface distance d of 20, 35, 50, 65, and 80 nm (spacing is defined as the surface to surface distance between adjacent disks).

center of the excitation beam. Assuming perfect alignment between the center of the excitation field and the center of the structure only modes with C_6 symmetry will be excited. This is in contrast to linear polarization illumination, which excites modes with mirror symmetry. Another characteristic of radial and azimuthal polarization illumination is that the transverse (x,y) energy density at the center is zero, because of the change in sign that the transverse fields undergo from $-(x,y)$ to $+(x,y)$. Therefore, for nanoscale disks, one should not

expect a significant difference between heptamer and hexamer structures under azimuthally and radially polarized light excitation. Additional theoretical and experimental aspects regarding the excitation of plasmonic clusters with high symmetry cylindrical vector beams are described in refs. 22 and 23.

With these observations in mind, we calculated the normalized extinction as a function of the wavelength of excitation (Figure 2) and the fields distributions at specific wavelengths of interest (Figure 3) using a full

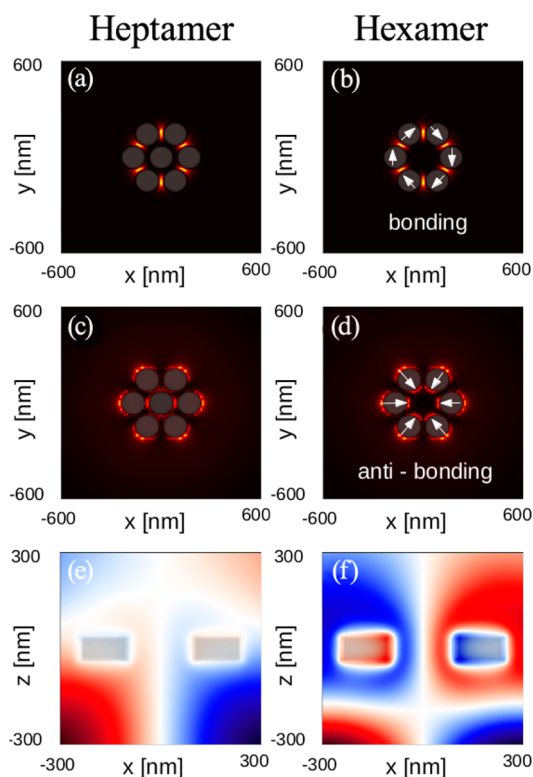


Figure 3. Transverse electric energy density, for (a and b) azimuthally polarized illumination, at the wavelength of $\lambda = 1110$ nm and (c and d) radially polarized illumination, at the wavelength of $\lambda = 700$ nm. Panels a and c were calculated for the heptamer configuration, while panels b and d were calculated for the hexamer structure. Panels e and f show a cross section of the azimuthally polarized field along $y = 0$ of the hexamer structure, which is illuminated from the bottom by azimuthally polarized light at the wavelengths of 1410 and 1110 nm, respectively. All panels were calculated for oligomer spacing of 20 nm (spacing is defined as the gap between adjacent disks).

3D finite difference time domain (FDTD) code.²⁴ The disk radius was taken as 75 nm, and each disk height was 80 nm. The extinction is defined as $(1 - T)$ where T is the normalized transmission. The radially and azimuthally polarized illuminations are modeled as radially and azimuthally electric current sources, respectively, with beam radius of 800 nm, located 710 nm above the oligomers. First, we note from Figure 2 that the spectrum of both hexamer and heptamer structures is very similar for both azimuthally and radially polarized light excitation. This is consistent with the profile of the transverse energy density being essentially zero at the center. Therefore, the absence or presence of the central nanodisk has only a negligible impact for azimuthally and radially polarized light excitation.

For azimuthally polarized light, the results show a pronounced dip in extinction. We also note that the spectrum is red-shifted when decreasing the spacing between the oligomers. This is because each disk can be considered as a dipole which is almost aligned with its two neighboring peripheral disks (see white arrows in Figure 3b). Bringing the disks closer together bonds

the dipoles and lowers the energetic state. At this wavelength, a collective mode is excited with its phase opposite to the illumination phase, as can be seen in Figure 3f. Thus, the illumination and the excited mode interfere destructively, diminishing the radiative damping. In contrast, for a wavelength outside of this dip in extinction (see Figure 3e) the phase of the excitation mode is very similar to the phase of the near field around the oligomers.

For linear polarization illumination, a dip is clearly observed around $\lambda = 750$ –800 nm for the heptamer structure, while this dip is absent for the hexamer. This is consistent with earlier work which has demonstrated that the presence of the central disk changes the field distribution dramatically at specific wavelengths for which a subradiant mode is excited, and interferes destructively with the superradiant dipolar mode.^{4–7} This type of interference is also known as a Fano resonance.²

For radially polarized illumination, it is observed that changing the oligomer spacing does not change the spectrum as dramatically as for the azimuthal and linear polarization cases. Yet, a small shift can still be observed, in the direction opposite to the previous case of azimuthally polarized light. This result can be explained by observing the transverse energy density in Figure 3c, 3d. As can be seen, in contrast to the case of azimuthally polarized light excitation, the energy density is not localized between the closely spaced oligomers, thus effectively reducing the near-field interaction between adjacent disks. In contrast to the case of azimuthally polarized light, for radially polarized illumination every two adjacent peripheral disks have almost parallel dipoles (see white arrows in Figure 3d), and therefore, the energy of this state rises with decreasing the disk spacing.^{2,25}

Figure 4 shows the energy levels and the polarization dependence, as well as schematic drawings of the optical spectra for heptamer and hexamer structures (left and right columns, respectively). The red framed states are actually the ones that are observed in the experiment.

Figure 4a depicts the situation for radial polarization. Considering only radially inward and outward directed dipoles, the ground state corresponds to alternatively arranged dipoles that point away or toward the center. Both the hexamer and heptamer exhibit the same behavior. Both modes cannot be excited by linearly polarized light at all as the net-dipole moment, given as the sum over all individual dipole moments, is zero. Yet, interestingly the energetically higher mode is perfectly matched to the polarization field of a radially polarized light field and is therefore excited with a very high efficiency. In this case, both for the hexamer and for the heptamer, the individual dipoles point radially outward—hence the neighboring dipoles repel each other and lead to a higher energy of this state. Hence, the excited state is the one that can be observed under normally incident radially polarized light (depicted at

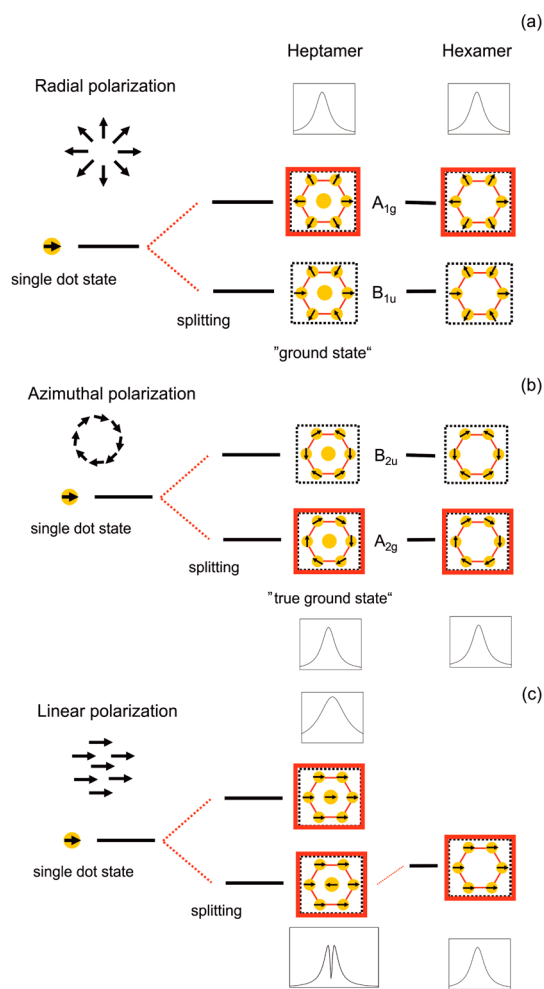


Figure 4. This figure shows the different modes and schematic absorption spectra for radial and azimuthal, as well as linear incident polarization at normal incidence angle. In the left, the polarization is schematically displayed. The plasmon hybridization (energy axis in y -direction) is shown for the heptamer and hexamer structures. Dipole allowed modes are displayed with a red frame. The “true ground state” is the ground state that is dipole allowed and can therefore be excited by azimuthally polarized light.

the upper left of the top panel of Figure 4), and this mode can be observed in absorption, which results in absorption peak for these levels (depicted next to the excited states above the dipole arrangement images).

Figure 4b illustrates the situation for azimuthally polarized light. In this case, the ground state arrangements, both for hexamer and heptamer, feature longitudinally arranged dipoles that line up in the tip-to-end ordering. Hence, the positive and negative net charges attract each other and lead to a reduced Coulomb repulsion and hence a lower energy. Absorption resonances (depicted below the schematic arrangements) can be observed, as the electric field (depicted on the upper left side of the middle panel of Figure 4) perfectly matches the dipolar arrangement. The excited state with antisymmetric longitudinal ordering features a higher energy, but cannot be excited at normal incidence by dipolar transitions.

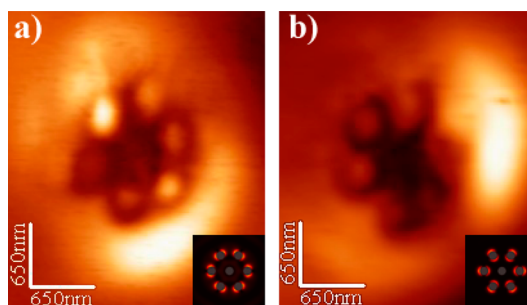


Figure 5. Near-field measurements showing intensity distribution around the heptamer under (a) azimuthally and (b) radially polarized excitation. The insets show the transverse energy density calculated for the specific dimensions of the measured sample at the excitation wavelength of 980 nm.

It is noteworthy that in both cases for radial and azimuthal polarization, there is no fundamental difference for hexamers and heptamers. This is radically different in the case of linear polarization, demonstrated in the bottom panel of Figure 4. This Electromagnetically Induced Transparency (EIT) case for the plasmonic oligomer has been discussed in detail by Nordlander⁴ as well as by Hentschel.^{6,26} In this case, the hexamer and heptamer behave differently. Whereas the hexamer shows only a superradiant mode, where all dipoles are aligned along one direction, the heptamer shows a complex spectral structure, where a broad superradiant resonance interferes destructively with a dark resonance with a counter-aligned dipole in the center. In the hexamer structure this center is missing and hence the EIT-like dip is not possible. In principle, one could also think of a dark hexamer mode at much higher energy, where the dipoles are aligned in anti-parallel fashion (not shown in this panel).

To observe experimentally the mode distribution around the oligomers, we performed near-field measurements using a near-field scanning optical microscope (NSOM, see Methods). Figure 5a,b shows the near-field response of a heptamers under azimuthally and radially polarized light excitation, respectively. To facilitate the NSOM measurement, we used a slightly larger sample with a disk radius of 130 nm and a spacing of 280 nm. Overall, the measurements follow the trend predicted by the simulation; *i.e.*, there is enhancement in energy density in the vicinity of each disk, except for the central one. However, we can hardly observe the specific field distribution around each disk, for reasons that are explained in the next section. Additionally, the measured signal is not circularly symmetric. This is because of the probe properties. Normally, bended probes have higher transmission efficiency for polarization perpendicular to the bending axis. Therefore, the tip, in addition to its capability of collecting the near-field signal, acts also as a polarizer. For this reason, two lobes are observed for the excitation beam, and the orientation of these lobes is rotated by 90° when the excitation polarization is switched from azimuthal to

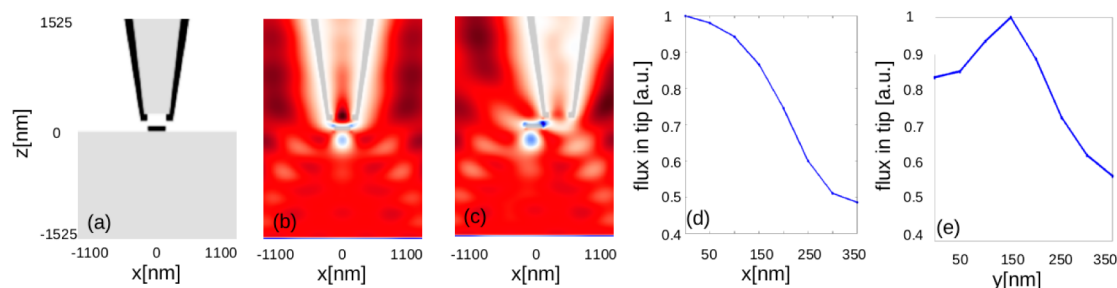


Figure 6. (a) Schematic description showing a cross section the NSOM probe on top of a single disk. The gray region represents glass, and black regions are the Au coating of the NSOM probe and the single disk. (b and c) Longitudinal Poynting vector (S_z) distribution for the case of zero and 350 nm lateral shift, respectively. Illumination is originated from the bottom, and red indicates power flux going upward, while blue indicates the downward direction. (d and e) Normalized power flux collected by the NSOM probe as a function of the lateral shift between the disk and the probe.

radial. This effect is also helpful in assessing the alignment between the excitation beam and the sample.

To better understand the interaction of the NSOM probe with the near field, we performed a full-3D FDTD simulation describing the scenario of light propagation near a single disk with an aperture tip located on top of it. To match our experimental data, the disk radius was assumed to be of 130 nm, and its thickness was 80 nm. Below is a glass substrate with refractive index $n = 1.45$, and illumination is from below with illumination, linearly polarized light in the y -direction. The probe is assumed to be coated with Au and its aperture diameter is 250 nm (see schematic in Figure 6a). We have calculated the Poynting vector in the longitudinal direction (representing the intensity of the signal propagating in the NSOM probe) as a function of the lateral shift between the disk and the probe (measured from the center of the tip to the center of the disk). The results (Figure 6d) show a monotonic decrease in intensity as a function of the shift, with maximal signal being collected when the probe is positioned on top of the disk. Two representative cases showing the longitudinal Poynting vector distribution for the case of zero and 350 nm lateral shift are shown in Figure 6, panels b and c, respectively. These figures provide a visual indication for the drop in collection efficiency of the NSOM probe as it is shifted from the center of the disk. One should note that an accurate prediction of probe-light interaction is a challenging task. For

example, the simulation assumes an ideal cylindrically symmetric shape for the NSOM probe, while in reality our NSOM probes are not perfectly smooth and not perfectly symmetric as assumed. Nevertheless, we believe that the simulation still provides a reasonable explanation for the measured NSOM results, demonstrating higher energy localization in the center of each disk, rather than at its boundaries, as one would naively anticipate by observing the field distributions.

CONCLUSIONS

In conclusion, we have studied theoretically and experimentally the interaction of plasmonic oligomer structures with spatially varying polarization illumination. The radially and azimuthally polarized excitation was shown to excite the highly symmetric modes of the hexamer and the heptamer structures. In contrast, linearly polarized illumination results in modes with a lesser degree of symmetry. Remarkably, no Fano resonances are observed for both hexamer and heptamer structures under radially and azimuthally polarization excitation, as expected from the absent dark mode in this case. Near-field scanning measurements have shown significant enhancement of the electric field energy density around the oligomers. The demonstrated capability of tailoring the response of oligomer structures by controlling not only their geometry but also the polarization of excitation may open new avenues toward further enhancement and control of light matter interaction on the nanoscale.

METHODS

The structures were defined on a glass substrate by electron beam lithography in a positive resist (PMMA) followed by thermal evaporation of a 3 nm Cr adhesion layer and 80 nm gold followed by a lift-off procedure. The footprint of each array is $100 \times 100 \mu\text{m}^2$. The thickness of all the particles is 80 nm. Three-dimensional simulations are employed to calculate the extinction and near-field distributions by using an open-source freely available finite-difference-time-domain code (MEEP, see ref 24). The NSOM measurements were conducted using a commercial system (Nanonics MultiView 4000). The sample was illuminated from below at the wavelength of 980 nm (using a diode laser) by a $100\times$ microscope objective, and the transmitted signal was

collected from the top using a metal-coated NSOM probe with an aperture diameter of 250 nm. Before it was focused onto the sample, the linearly polarized beam emerging from the laser was converted to a radially/azimuthally polarized beam with the aid of a liquid crystal converter (ARCOptix S.A, Switzerland).

Conflict of Interest: The authors declare no competing financial interest.

Acknowledgment. This research was supported by a Grant from the GIF, the German-Israeli Foundation for Scientific Research and Development, as well as an ERC Advanced Grant (COMPLEXPLAS).

REFERENCES AND NOTES

- Stockman, M. I. Nanoplasmonics: Past, Present, and Glimpse into Future. *Opt. Express* **2011**, *19*, 22029.
- Halas, N. J.; Lal, S.; Chang, W.-S.; Link, S.; Nordlander, P. Plasmons in Strongly Coupled Nanostructures. *Chem. Rev.* **2011**, *111*, 3913–3961.
- Luk'yanchuk, B.; Zheludev, N. I.; Maier, S. A.; Halas, N. J.; Nordlander, P.; Giessen, H.; Chong, C. T. The Fano Resonance in Plasmonic Nanostructures and Metamaterials. *Nat. Mater.* **2010**, *9*, 707–715.
- Mirin, N. A.; Bao, K.; Nordlander, P. Fano Resonances in Plasmonic Nanoparticle Aggregates. *J. Phys. Chem. A* **2009**, *113*, 4028–4034.
- Fan, J. A.; Wu, C.; Bao, K.; Bao, J.; Bardhan, R.; Halas, N. J.; Manoharan, V. N.; Nordlander, P.; Shvets, G.; Capasso, F. Self-Assembled Plasmonic Nanoparticle Clusters. *Science* **2010**, *328*, 1135–1138.
- Hentschel, M.; Saliba, M.; Vogelgesang, R.; Giessen, H.; Alivisatos, A. P.; Liu, N. Transition from Isolated to Collective Modes in Plasmonic Oligomers. *Nano Lett.* **2010**, *10*, 2721–2726.
- Lassiter, J. B.; Sobhani, H.; Fan, J. A.; Kundu, J.; Capasso, F.; Nordlander, P.; Halas, N. J. Fano Resonances in Plasmonic Nanoclusters: Geometrical and Chemical Tunability. *Nano Lett.* **2010**, *10*, 3184–3189.
- Frimmer, M.; Coenen, T.; Koenderink, A. F. Signature of a Fano-Resonance in a Plasmonic Meta-Molecule's Local Density of Optical States. *Phys. Rev. Lett.* **2012**, *108*, 077404.
- Rahmani, M.; Lei, D. Y.; Giannini, V.; Lukiyanchuk, B.; Ranjbar, M.; Liew, T. Y. F.; Hong, M.; Maier, S. A. Subgroup Decomposition of Plasmonic Resonances in Hybrid Oligomers: Modeling the Resonance Lineshape. *Nano Lett.* **2012**, *12*, 2101–2106.
- Lassiter, J. B.; Sobhani, H.; Knight, M. W.; Mielczarek, W. S.; Nordlander, P.; Halas, N. Designing and Deconstructing the Fano Lineshape in Plasmonic Nanoclusters. *Nano Lett.* **2012**, *12*, 1058–1062.
- Ogüt, B.; Talebi, N.; Vogelgesang, R.; Sigle, W.; van Aken, P. A. Toroidal Plasmonic Eigenmodes in Oligomer Nanocavities for the Visible. *Nano Lett.* **2012**, *12*, 5239–5244.
- Zhan, Q. Cylindrical Vector Beams: from Mathematical Concepts to Applications. *Adv. Opt. Photonics* **2009**, *1*, 1–57.
- Youngworth, K.; Brown, T. Focusing of High Numerical Aperture Cylindrical-Vector Beams. *Opt. Express* **2000**, *7*, 77–87.
- Dorn, R.; Quabis, S.; Leuchs, G. Sharper Focus for a Radially Polarized Light Beam. *Phys. Rev. Lett.* **2003**, *91*, 233901.
- Lerman, G. M.; Levy, U. Effect of Radial Polarization and Apodization on Spot Size under Tight Focusing Conditions. *Opt. Express* **2008**, *16*, 4567–4581.
- Chen, W.; Zhan, Q. Realization of an Evanescent Bessel Beam via Surface Plasmon Interference Excited by a Radially Polarized Beam. *Opt. Lett.* **2009**, *34*, 722–724.
- Lerman, G. M.; Yanai, A.; Levy, U. Demonstration of Nanofocusing by the use of Plasmonic Lens Illuminated with Radially Polarized Light. *Nano Lett.* **2009**, *9*, 2139–2143.
- Brandl, D. W.; Mirin, N. A.; Nordlander, P. Plasmon Modes of Nanosphere Trimers and Quadrumers. *J. Phys. Chem. B* **2006**, *110*, 12302–12310.
- Bao, K.; Mirin, N. A.; Nordlander, P. Fano Resonances in Planar Silver Nanosphere Clusters. *Appl. Phys. A: Mater. Sci. Process.* **2010**, *100*, 333–339.
- Jäger, S.; Kern, A. M.; Hentschel, M.; Jäger, R.; Braun, K.; Zhang, D.; Giessen, H.; Meixner, A. Au-Nanotip as Luminescent Near-Field Probe. *Nano Lett.* **2013**, *13*, 3566–3570.
- Hentschel, M.; Dorfmueller, J.; Giessen, H.; Jäger, S.; Kern, A. M.; Zhang, D.; Meixner, A. J. Plasmonic Oligomers in Cylindrical Vector Light Beams. *Beilstein J. Nanotechnol.* **2013**, *4*, 57–63.
- Sancho-Parramon, J.; Bosch, S. Dark Modes and Fano Resonances in Plasmonic Clusters Excited by Cylindrical Vector Beams. *ACS Nano* **2012**, *6*, 8415–8423.
- Gomez, D. E.; Teo, Z. Q.; Altissimo, M.; Davis, T. J.; Earl, S.; Roberts, A. The Dark Side of Plasmonics. *Nano Lett.* **2013**, *13*, 3722–3728.
- Oskooi, A. F.; Roundy, D.; Ibanescu, M.; Bermel, P.; Joannopoulos, J. D.; Johnson, S. G. MEEP: A Flexible Free-Software Package for Electromagnetic Simulations by the FDTD Method. *Comput. Phys. Commun.* **2010**, *181*, 687–702.
- Lassiter, J. B.; Aizpurua, J.; Hernandez, L. I.; Brandl, D. W.; Romero, I.; Lal, S.; Hafner, J. H.; Nordlander, P.; Halas, N. J. Close Encounters Between Two Nanoshells. *Nano Lett.* **2008**, *8*, 1212–1218.
- Hentschel, M.; Dregely, D.; Vogelgesang, R.; Giessen, H.; Liu, N. Plasmonic Oligomers: The Role of Individual Particles in Collective Behavior. *ACS Nano* **2011**, *5*, 2042–2050.